

i-WiViG: Interpretable Window Vision GNN

Ivica Obadic^{1,2*} Dmitry Kangin^{3,4†} Dario Oliveira⁵
Plamen P Angelov^{3†} Xiao Xiang Zhu^{1,2}

¹Technical University of Munich ²Munich Center for Machine Learning
³University of Lancaster ⁴University of Manchester ⁵Getulio Vargas Foundation

Abstract

Deep learning models based on graph neural networks have emerged as a popular approach for solving computer vision problems. They encode the image into a graph structure and can be beneficial for efficiently capturing the long-range dependencies typically present in remote sensing imagery. However, an important drawback of these methods is their black-box nature which may hamper their wider usage in critical applications. In this work, we tackle the self-interpretability of the graph-based vision models by proposing our Interpretable Window Vision GNN (i-WiViG) approach, which provides explanations by automatically identifying the relevant subgraphs for the model prediction. This is achieved with window-based image graph processing that constrains the node receptive field to a local image region and by using a self-interpretable graph bottleneck that ranks the importance of the long-range relations between the image regions. We evaluate our approach to remote sensing classification and regression tasks, showing it achieves competitive performance while providing inherent and faithful explanations through the identified relations. Further, the quantitative evaluation reveals that our model reduces the infidelity of post-hoc explanations compared to other Vision GNN models, without sacrificing explanation sparsity.

1. Introduction

Many existing pattern recognition methods, applied to image data, prioritize the texture of the image over the composition [7]; in particular, it can manifest in the form of a Picasso problem [21] where the relative position of elements does not matter as much as their texture. In many remote sensing problems, however, this may cause a problem as often rela-

tions between the patches of image data are equally or more important than the texture [14]. Furthermore, it makes it important to explain such decision-making in terms of long-range spatial dependencies between the nodes of a graph.

One promising direction towards solving this problem is based on encoding the image into a graph structure. Notably, works such as Vision GNN (ViG) [8, 9, 16, 17, 25] combine texture-based patch extraction with high-level graph representation learning. These approaches are getting increasingly used for remote sensing applications such as land-cover change detection and classification [23, 24, 32, 36] or anomaly detection after a natural hazard [3]. However, despite their capability to efficiently model the long-range interactions within an image, we found that ViG approaches typically yield large and overlapping receptive fields that prevent the attribution of the graph nodes to individual patches in the input image. This is illustrated in Figure 1.1a, through the example of the blue and the pink nodes that lie on the opposite ends of the image, yet are connected via the global k -nearest neighbor graph. Consequently, as depicted in 1.1b, even after a single layer of graph processing, the receptive fields of these two nodes disperse across the entire image and become highly overlapping (the lavender color visualizes their overlap). In addition to their lack of inherent interpretability, the inability to relate nodes to local patches in the image disables the application of the common graph explanation approaches such as GNNExplainer [31] to the ViG models and therefore reduces their interpretability only to post-hoc vision explanation methods such as saliency maps that are of limited faithfulness [1]. To overcome these issues and achieve inherent ViG interpretability, we propose our i-WiViG approach visualized in the bottom row of Figure 1. Our approach relies upon the local window graph processing [25] to constrain the receptive field of the node in the graph to a smaller and contiguous patch in the image (visualized in Figures 1.2a and 1.2b). Next, it inserts an interpretable Graph Neural Networks (GNN) bottleneck responsible for encoding the global long-range dependencies in the image (Figure 1.2c). The graph bottleneck is based on the stochastic attention mechanism [15] that constrains the

*The work began during the author’s research visit to the University of Lancaster supported by TAILOR, a project funded by EU Horizon 2020 research and innovation programme under Grant Agreement No. 952215.

†The work has been developed with the support of European Union’s ELSA – European Lighthouse on Secure and Safe AI, Horizon Europe, Grant Agreement No. 101070617.

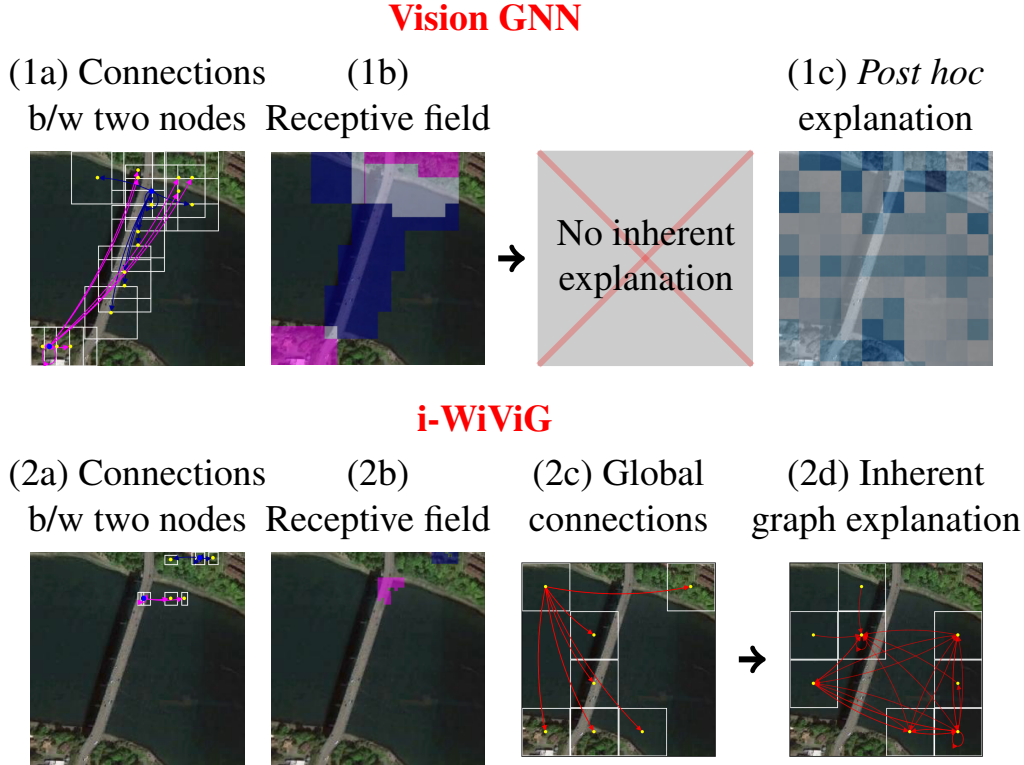


Figure 1. VisionGNN approaches visualized in the top row yield large and overlapping receptive fields for the graph nodes, which limits their interpretability only to the standard vision post-hoc attribution methods such as saliency maps. In contrast, our i-WiViG approach depicted in the bottom row offers an inherently interpretable model that relies on local window graph processing to constrain the node receptive field and further introduces an interpretable graph bottleneck that learns a ranking of the long-range dependencies between the local windows that inherently explain the model workings. Such explanations cannot be obtained through the Vision GNN (ViG) models.

model prediction to rely on the estimated edge importance. As a result, our approach automatically reveals the relevant subgraph for the outcomes during inference time (1.2d).

In summary, our work provides the following main contributions:

- We propose a novel and inherently interpretable ViG approach for remote sensing classification and regression tasks, called i-WiViG that combines local window graph processing with an inherently interpretable graph bottleneck approach that automatically learns to rank the relations between the local image patches.
- We qualitatively and quantitatively analyze the identified subgraphs with our method and illustrate that it reliably explains the critical long and short-range dependencies for the model inference.
- Our extensive quantitative evaluation reveals that our method reduces the infidelity and does not decrease the sparsity of post-hoc explanations compared to the other ViG methods.

2. Related Work

Graph Neural Networks for Computer Vision The recent approaches for solving computer vision tasks with graph neural networks [8, 9, 16, 17, 25] consist of the following three steps: (1) extracting graph nodes from the input image with the stem operation, (2) constructing the graph adjacency matrix, and (3) performing graph message passing to derive the outcome. The stem operation extracts graph nodes from the image by applying a series of convolutional layers that transform the input image into a high-level feature map. The pixels in this feature map are encoded into graph nodes that cover rectangular patches in the input image. Next, the edges are added with the k -nearest neighbors search based on the node embedding in the feature map. Finally, the constructed graph is processed with a GNN to predict the image label. The ViG approaches were introduced in the pioneering work of Han et al. [8] which defines two ViG architectures: isotropic ViG and pyramid ViG. The isotropic architecture is analogous to the Vision Transformers (ViT) as it keeps the features with equal size and shape throughout the network. In contrast, the pyramid architecture gradually

Table 1. Comparison between different models of the ViG family: our model is the only one providing both local and global receptive fields; we prevent overlap between the nodes by choosing kernel size/stride 2/2 instead of 3/2 which is common in the ViG models, and our model is the first one which is self-interpretable.

Model	ViG [8]	Vision HGNN[8]	Mobile ViG [16]	GreedyViG[16]	WiGNet [25]	i-WiViG(ours)
Receptive field	Global	Global	Global	Global	Local	Local + Global
Kernel size/stride	✗	3 / 2	3 / 2	3 / 2	3 / 2	2 / 2
Self-interpretable	✗	✗	✗	✗	✗	✓

reduces the spatial size while increasing the feature dimensionality as the image traverses through the network. This is achieved by alternating between graph layers that perform the message passing and convolutional layers that downsample the spatial size of the feature maps while increasing the feature dimensionality. The follow-up works typically focus on improving the graph representation and addressing the computational bottleneck of the k -nearest neighbor search for defining graph edges [9, 16, 17, 25]. In detail, Han et al. [9] note that edges in the ViG model encode only pairwise relationships between the patches which limit the model’s capability to capture the high-order interactions in an image and yields redundant edges. To overcome this, the authors introduce the Vision HGNN model that encodes the image as a hypergraph and relies on a hypergraph convolutional layer for message passing. The computational burden of the k -nearest neighbor graph is further tackled by Munir et al. in the MobileViG model which constructs a static graph independent of the input image by connecting a node with every second node in its row and column of the feature map [16]. In their follow-up work, the authors propose the GreedyViG model that employs a dynamic graph construction procedure [17]. First, it estimates the Euclidian distance between the diagonal image quadrants and then connects nodes in the same row and column within one standard deviation from the average distance of the diagonal image quadrants. A unique property of the aforementioned approaches is the k -nearest neighbor search is not constrained to a local vicinity of the node positions, which as visualized in Figure 1b, results in global, and typically overlapping node receptive fields. In contrast, the recent work of Spadaro et al. introduces a pyramid Windowed Vision Graph Neural Network (WiGNet) model that limits the search of k -nearest neighbors and the graph processing to local windows in the image [25].

As summarized in Table 1, the above state-of-the-art ViG models can mainly be distinguished based on their receptive field to global [8, 9, 16, 17] or local [25]. However, all of them are black-box models as they do not automatically provide insights into their decision mechanism and can only be explained with vision post-hoc approaches such as saliency maps that are of questionable reliability [1]. We address this problem by proposing an inherently interpretable ViG that explains the model working by constraining the node recep-

tive field to a local image patch and using a graph bottleneck to reveal the critical interactions for the model prediction by learning to rank the relations between the image patches.

GNN Explainability The existing methods for GNN explainability often aim to identify the relevant nodes and edges in the graph for prediction. These methods can be split into two categories: *post hoc* and *ante hoc* methods. The *post hoc* methods aim to explain a trained graph neural network. One of the most popular graph explanation methods in this category is the GNNExplainer [31], which identifies the relevant subgraph by maximizing mutual information between the predicted label distribution and the explanatory subgraph. [33] instead takes a holistic approach towards *post hoc* interpretability, generating the largest output inputs of a given size for each class. As another example, [13] creates a causal explanation by maximizing the information flow measurements. However, a main drawback of the *post hoc* approaches is that they usually do not come with strict guarantees for the fidelity of the explanations to the actual working of the model on which they operate [22, 34]. The nascent area of *ante hoc* graph interpretation methods aims at proposing the architecture that propagates, by design, the attribution to the nodes and edges as a part of the decision-making. For instance, the Graph Stochastic Attention (GSAT) approach [15] by Miao et al. constrains the model prediction to rely on the automatically learned edge weights and uses the notion of stochasticity to ensure that the edges relevant to the inference have a high weight. Another example is the work of Scafarto et al. [22] that studies the potential for using the data augmentations for identifying the parts of the graph that contribute towards the decision. Further, Chen et al. [4] use a combinatorial optimization technique, called multilinear extension, to find out the subgraphs that matter for the decision-making process.

3. Preliminaries

We define a graph $G(V, E) \in \mathbb{G}$, where V are the vertices and E are the edges of the graph, and \mathbb{G} is the set of possible graphs. We consider the task of prediction of label mapping from the graph to the vector labels $y(\cdot) : \mathbb{G} \rightarrow \mathbb{L}$, where $\mathbb{L} \subset \mathbb{R}^{k_{\mathbb{L}}}$ and $k_{\mathbb{L}}$ is the size of the output vector.

3.1. Preliminaries: Vision GNN model

Vision GNN Our work builds upon the Vision GNN (ViG) [8] and Windowed Vision Graph Neural Network (WiGNet) [25] architectures, which leverage graph representation learning from patchwise image embeddings. In the first step, these approaches apply the *stem* layer which includes a series of convolutional layers to divide the image into patches, each covering a rectangular part of the image. Each patch encodes a node in the image and in the next step, a k -nearest neighbors adjacency matrix is formed based on the node embeddings. ViG offers two architectures, namely *isotropic* and *pyramid*. In the isotropic architecture, the number of nodes and their feature size is kept constant throughout the network while the pyramid architecture gradually decreases the number of nodes with downsampling operations in a way similar to the ResNet architecture [10]. The ViG network defines the *Grapher* module that uses the graph convolutional layers of the following form

$$G' = \text{Update}(\text{Aggregate}(G, \mathbf{w}_a), \mathbf{w}_u), \quad (1)$$

where *Update* and *Aggregate* are the update and aggregation operators parameterised with the weights \mathbf{w}_a and \mathbf{w}_u respectively, G is an input graph and G' is the output graph. To increase the feature diversity, the *Grapher* module introduces a linear layer before and after the graph convolution and similar to the ViT model, processes the features of each node in a feed-forward network. To enable training of deep architectures, [8] dynamically recomputes the k -neighbours adjacency matrix based on the output of the *Grapher* layer. These operations result in a global receptive field of the graph nodes dispersed across the different parts of the image.

Windowed Vision Graph Neural Network (WiGNet) In contrast to the other ViG approaches, the WiGNet model [25] introduced by Spadaro et al. limits the graph nodes to local regions in the image. This is achieved by grouping the patches from the stem operation into windows and afterward computing the k -nearest neighbor graph and the above *Grapher* layer from ViG, locally, within each window. The WiGNet has a pyramid architecture and similar to ViG, it dynamically computes k -nearest neighbor adjacency matrix after each block of *Grapher* and downsampling layers.

3.2. Graph Stochastic Attention (GSAT)

The Graph Stochastic Attention (GSAT) approach proposed by Miao et al. [15] is a self-interpretable graph neural network that learns to automatically select the relevant subgraph during the model inference. Along with the model prediction, GSAT outputs estimated edge weights describing the explanation subgraph. It is an approach rooted in the graph information bottleneck principle [28] that identifies a subgraph G_S from the input graph G capable of accurately

predicting the target label Y . To identify the subgraph, the GSAT approach learns an attention distribution α over the graph edges by injecting stochasticity during training. In detail, the GSAT approach first estimates the probability p_{uv} of sampling the edge (u, v) that is afterward used as the weight for the edge in the forward pass. The edge embedding is constructed by concatenating the embeddings of the node u and the node v and it is passed through a series of FFN layers that output p_{uv} . Next, during training, a Bernoulli sampling is performed for each edge (u, v) using p_{uv} as a sampling probability. This enforces the model to output high weight to the relevant edges so that there is a high probability that these edges are selected in the resulting subgraph. Thus, the highest p_{uv} values indicate the critical edges for the model prediction. In practice, the GSAT approach is implemented by injecting a random noise during training to the estimated edge weights and by introducing hyperparameter r that regularizes the edge weights with the following loss function: $\mathcal{L} = \mathcal{L}_{\text{task}} + \mathcal{L}_\alpha$, with

$$\mathcal{L}_\alpha = \sum_{(u,v) \in E} p_{uv} \log \frac{p_{uv}}{r} + (1 - p_{uv}) \log \frac{1 - p_{uv}}{1 - r} \quad (2)$$

The hyperparameter r controls the distribution of the edge weights and makes \mathcal{L}_α term minimal when all edge weights are equal to r . At the same time, in case a subset of the edges bears the critical information for the model prediction, the task loss term will force those critical edges to have weights higher than r . Hence, the edges with the highest weight can be used to uncover the critical subgraph to model the prediction.

4. Method

In this paper, we propose i-WiViG (Interpretable Window Vision GNN), a self-interpretable ViG model (illustrated in Figure 2) that reveals the relevant subgraph for the model prediction during inference time. To achieve self-interpretability, our model addresses the limitations of global and overlapping receptive fields of the nodes in the ViG model and the lack of global connections in the WiGNet.

As illustrated in Section 3.1, the ViG model can connect a patch to any other patch in the image. Figure 1b depicts that even after a single layer of processing, the nodes in the graph start to have a large overlap in their receptive fields which makes it hard to attribute a node to a rectangular patch in the image. While the WiGNet addresses this problem by local window graph processing, it still fails to consider the long-range dependencies. To overcome these limitations, our proposed method consists of the following two main steps:

1. Restricting the node receptive field to a local image region.
2. Introducing a graph bottleneck to automatically rank the relevant relations between the image regions.

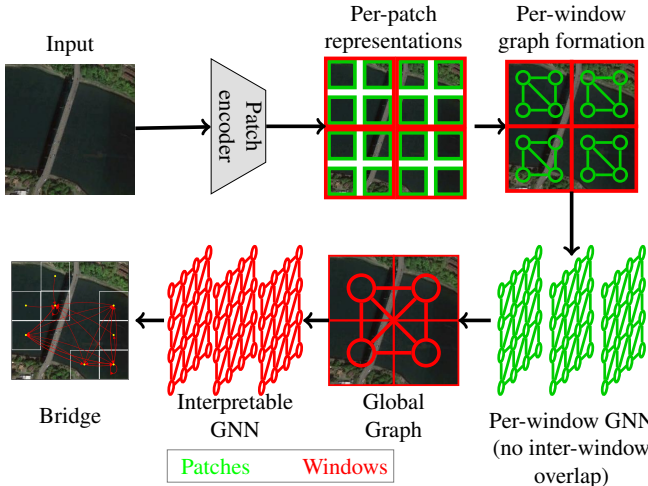


Figure 2. i-WiViG is split into several steps: (1) per-patch representation learning, (2) per-window graph formation, (3) graph representation learning for the window graphs (4) interpretable graph representation learning over the global graph, where the nodes represent windows. As an output, our model yields the prediction along with a ranking of the edge importance for the outcome.

For the first step, we rely on the WiGNet described in Section 3.1 to constrain the node receptive field to a local image patch. We adopt its pyramid ViG architecture by using three stages of local window processing followed by downsampling layers. In contrast to the WiGNet, we reduce the overlap between the node receptive fields and avoid information leakage by downsampling with a kernel size of 2 and stride 2 (similar to [26]). As a result of the previous operations, the nodes in the graph can be associated with a rectangular window/patch in the input image. In the second step, we model the long-range dependencies between the high-level representations of the image patches by constructing a k -nearest neighbors graph and feeding this graph to the GSAT model. Finally, the outputs of the GSAT model are the model prediction and edge weights that provide the model explanation in terms of the importance of the global connections between the windows in the image. The detailed architecture of our method is presented in Section A, Table 4 in the Appendix.

In Table 1, we provide a detailed comparison between the different members of the ViG family of methods. To the best of our knowledge, our i-WiViG approach is the first self-interpretable ViG method, which combines both, local and global receptive fields.

5. Experimental Setup

Datasets We evaluate our proposed model on the tasks of predicting class labels and regression outcomes from re-

mote sensing aerial imagery. For the classification task, we used the NWPU-RESISC45 dataset to classify 31,500 aerial images into 45 scene classes [5]. The images are of size 256×256 pixels and the dataset contains 700 images per class. We used the dataset splits provided in [19] that assign 60% of the instances into training, 20% in the validation set, and the rest 20% in the test set, respectively. For the regression task, we used the Liveability dataset where the instances associate aerial imagery covering a neighborhood area in the cities in the Netherlands with its liveability score [11]. It includes 51,781 labeled image patches of size 500×500 and covers 13 cities in the Netherlands. For our experiments, we resized the images to 256×256 pixels and used the geographically stratified splits as provided by the authors, which enable evaluating model generalization on unseen cities during model training.

Vision Benchmark Approaches As ViG benchmark models, we have evaluated the tiny architectures of the isotropic and pyramid ViG models in [8] as well as the tiny WiGNet model [25]. Further, we also compare our method against two CNN baseline approaches, namely Resnet18 [10] and the BagNet [2]. The BagNet model derives the prediction by processing each local image patch independently. As such, it can shed light on the relevance of texture learning as opposed to encoding long-range spatial relations. We used the default hyperparameter settings for every model and evaluated the BagNet version using 17×17 patch size.

Model Training All models were trained with the Cosine Annealing schedule using an initial learning rate of 0.0005 and weight decay of 0.03. The vision benchmark approaches were trained for 200 epochs while i-WiViG was trained for 400 epochs as it required more epochs to converge due to the induced stochastic attention mechanism. During training, we evaluated the model performance every 10 epochs on the validation set, and for testing, we chose the model with the best performance on the validation set. Further details about the training procedure are provided in Appendix, Section B.

6. Results

6.1. Model Performance

Table 2. Model performance on the test sets.

Approach	Model	RESISC45		Liveability	
		Accuracy	F1 Score	R^2	τ
CNN	BagNet	0.89	0.89	0.36	0.47
	ResNet-18	0.93	0.93	0.38	0.46
ViG	Isotropic ViG	0.94	0.94	0.4	0.47
	Pyramid ViG	0.94	0.94	0.42	0.49
	WiGNet	0.93	0.93	0.4	0.49
Ours	i-WiViG	0.91	0.91	0.46	0.5

Table 2 compares the performance of our i-WiViG model with the different CNN and ViG benchmark approaches. The results for the NWPU-RESISC45 scene classification dataset in the third column reveal that our self-interpretable i-WiViG approach achieves accuracy and F1 score of 0.91. As such, it yields competitive performance with the benchmark approaches that have an accuracy and F1 score of around 0.93 except the Bagnet which exhibits poorer performance with an accuracy of 0.89. Regarding the liveability task, the last column of Table 2 shows that our approach achieves an improvement of around 0.08 and 0.04 in the R^2 score over the ViG and the CNN baselines, respectively and yields comparable performance for the Kendall τ correlation metric. While the Kendall τ indicates that the different models produce a similar ranking of the liveability scores, from the R^2 we can deduce that our i-WiViG is more accurate in the fine-grained prediction of the actual liveability values.

6.2. Qualitative Analysis of the Relevant Subgraphs

In contrast to the existing ViG models that can only be interpreted with *post hoc* Explainable AI (xAI) methods, our approach has the advantage of being inherently interpretable as it relies on the GSAT graph to rank the relevant edges describing the global interactions between the local image patches. In Figure 3 we provide qualitative examples of the identified relevant subgraphs for the examples of the class *Bridge* (Figure 3.a), the class *Airplane* (Figure 3.b) and the class *Medium Residential Area*. Figure 3.a shows that our model identifies a subgraph connecting the central part of the bridge with the land and the water on both sides of the bridge. Further, Figure 3.b illustrates that for the example of the airplane class, our model identifies a sparse subgraph that identifies the long-range dependencies between the airplanes and also locally connects specific parts within an airplane (as depicted by the edge from the elevator to the wings for the bottom airplane). Similarly, our model considers long-range dependencies between the road on the top-left and bottom-right of the image and local relations between the houses in the central part of the image to predict the medium residential area class In Figure 3. Further to this, in Figure 4 we provide explanation examples for the regression task. On the left-hand side, we can see that the most important edges group the houses into a connected component linked to the water body and the trees for the prediction of a high livability value. For example with medium liveability (4.b), we can see that the model identifies connections from the residential areas to the road and vegetation. Finally, for the low liveability scenario on the right, the model focuses on connections between the densely built-up areas. In summary, these examples show that our approach is capable of revealing the critical local relations and the long-range dependencies for the model predictions.

6.3. Quantitative Explanation Evaluation

6.3.1. Edge Weights Importance

To quantitatively assess the quality of the explanations produced with our model, we evaluate the *insertion* metric presented in [20] that increasingly introduces features to the model based on their importance and measures their impact on the model performance. We test this metric by sequentially adding edges to an empty graph, ordered by their importance estimated with GSAT, in both, descending and ascending fashion. If the edge weights are related to the prediction, introducing the edges with supposedly high importance to the graph should result in a higher Area Under the Curve (AUC) compared to when edges with low importance are inserted first. The results of this experiment are visualized in Figures 5 and 6 which demonstrate that for both tasks, the edge weights faithfully explain the model workings as the addition of the edges with high importance (blue curve) yields a sharper improvement in the model performance compared to when edges with low importance are added (orange curve). This difference is particularly striking for the scene classification task, where adding the most important edges first yields an AUC of 0.82, a substantial improvement over the 0.71 AUC achieved by adding the least important edges first.

6.3.2. Impact of the Edge Weights regularization

As described in Section 3.2, the r hyperparameter in the GSAT is critical for regularizing the distribution of the edge importance. In this section, we evaluate how different values of r impact the standard deviation of the edge weights, and consequently relate to the model accuracy, and the explanation quality measured with the AUC metric. Table 3 shows that in contrast to the classification task, the edge weights for the regression typically have several orders of magnitude lower standard deviation and the explanation quality exhibits higher sensitivity to the choice of the r value with lower values linked to poorer explanation quality (see additional results in Appendix, Section C). Further, we observe that for both tasks the r values are positively correlated with the model performance. These results indicate that when our approach is used for predicting continuous regression values, careful tuning of the edge weight distribution regularizer r is required to ensure decent model performance and explanation quality.

6.3.3. Post-Hoc Explanations

To assess the explainability properties of our approach beyond a qualitative evaluation, we quantitatively evaluate the *post hoc* xAI attributions. In this experiment, we compare the attributions computed with the Integrated Gradients (IG) [27] and Occlusion xAI methods on the explanation quality properties of infidelity [30] and sparsity [6]. On the one hand, infidelity measures the effect of perturbing the relevant

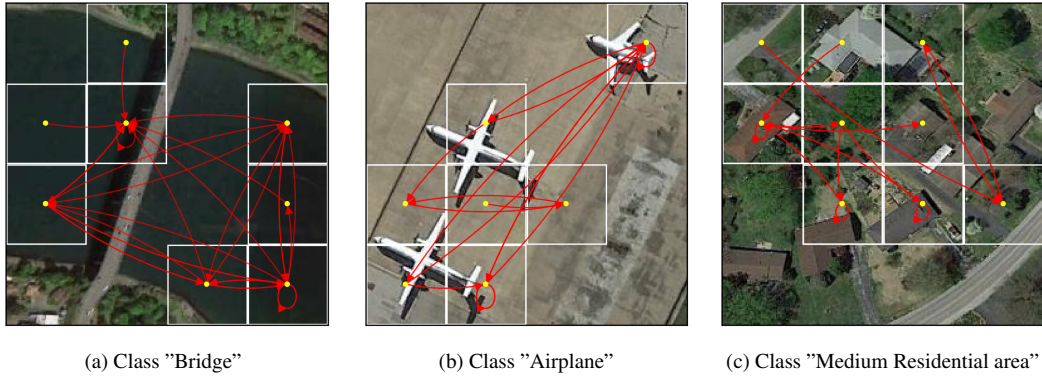


Figure 3. The relevant subgraphs within the top-5 edge importance percentile for the predictions of the i-WiViG model on examples of the class *Bridge* (left) and the class *Airplane* (middle) and *Medium Residential Area* (right) in the NWPU-RESISC45 dataset.

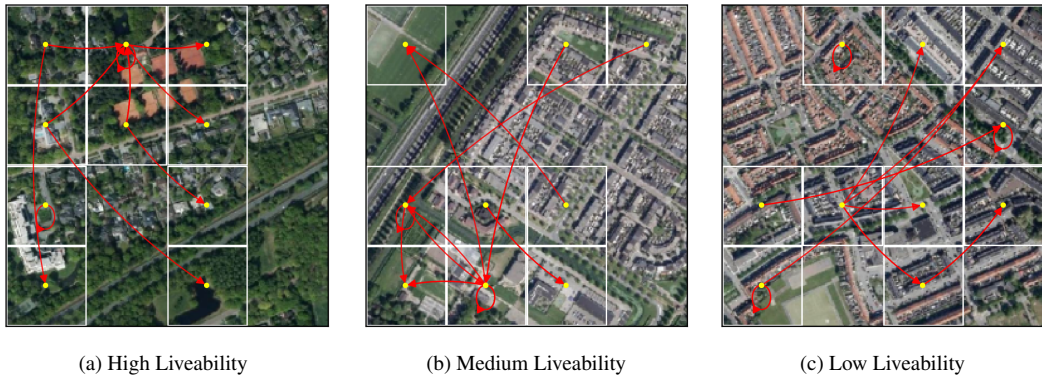


Figure 4. Examples of identified subgraphs containing edges within the top-5 importance percentile for the predictions of the i-WiViG model on examples of high (left), medium (centre) and low liveability areas (right) from the Liveability dataset.

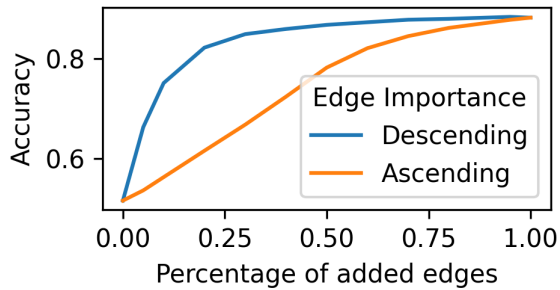


Figure 5. RESISC45 edge attribution evaluation after an incremental addition of the edges with highest importance (blue curve) and the edges with lowest importance (orange curve).

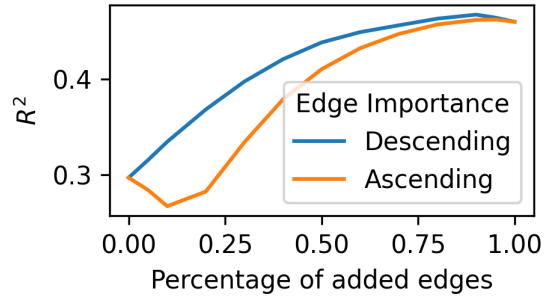


Figure 6. Liveability edge attribution evaluation after an incremental addition of the edges with highest importance (blue curve) and the edges with lowest importance (orange curve).

pixels in the image, as estimated by the xAI method, on the model predictions. Hence, explanations with low infidelity are preferred as this implies that model predictions change significantly when the relevant pixels are perturbed. On the other hand, the sparsity property evaluates the compact-

ness of an explanation and favors sparser explanations that identify a smaller subset of pixels in the image as relevant [18]. The results of this experiment on the test set of the NWPU-RESISC45 dataset are visualized in Figure 7. In detail, Figure 7.a illustrates that our i-WiViG model dras-

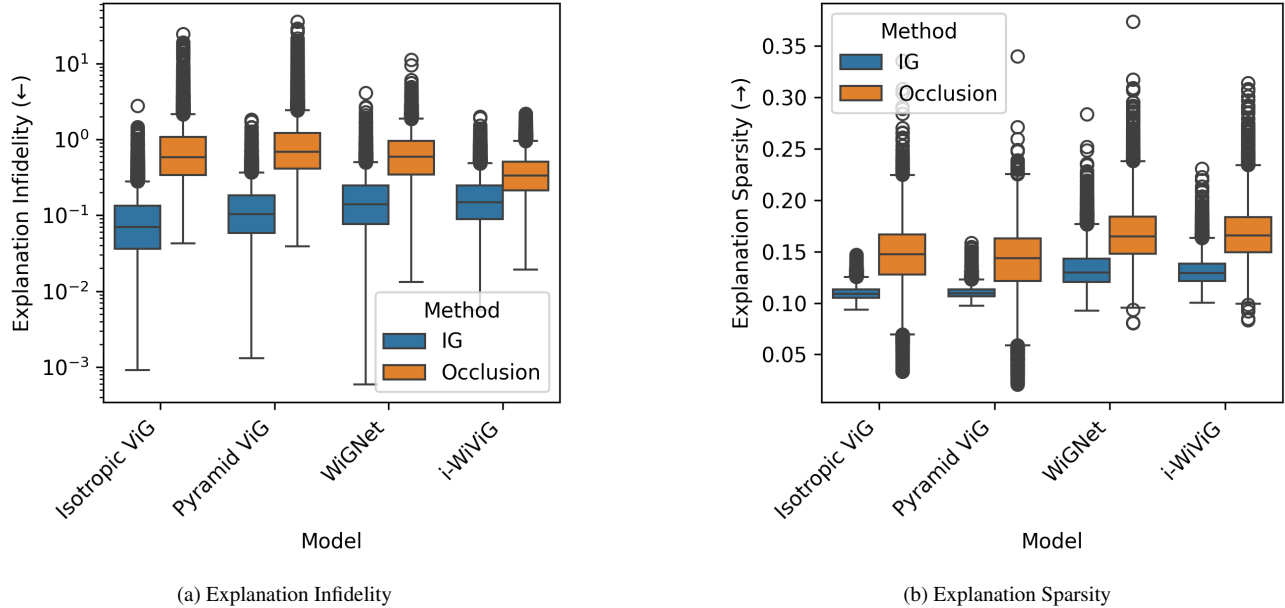


Figure 7. **Quantitative evaluation of the explanation quality of our method against the other Vision GNN benchmarks on the NWPU-RESISC45 scene classification dataset.** The left plot visualizes the explanation infidelity while the right plot depicts the explanation sparsity for the *post hoc* attributions computed with the Integrated Gradients (IG) and Occlusion methods. The arrows indicate the preferred directions for the metrics, i.e. explanations with low fidelity and high sparsity are preferred. The explanation infidelity is visualized on the log scale while the sparsity was computed according to the PQ index [6].

Table 3. Impact of r on the goodness of fit (shown are accuracy for classification and R^2 for regression) and explanation quality for classification and the regression tasks.

Dataset	GSAT r	Weights SD	Goodness of Fit	AUC
RESISC45	0.3	0.05	0.84	0.83
	0.5	0.07	0.89	0.86
	0.7	0.03	0.91	0.82
Liveability	0.3	0.02	0.29	0.15
	0.5	$6e^{-5}$	0.44	0.45
	0.7	$4e^{-4}$	0.46	0.41

tically reduces the number of outliers with high infidelity, particularly for the Occlusion attributions as it squashes the outliers towards the mean infidelity value. This results in the lowest infidelity on average for i-WiViG for the Occlusion attributions and comparable performance for the IG attributions. Similar trends can also be observed for the sparsity metric on the right plot in Figure 7 which shows that for both attribution methods, i-WiViG performs comparably to WiGNet as both models improve the explanation sparsity over the isotropic and pyramid ViG models. The similar results for the Liveability dataset are presented in Section D of the Appendix.

7. Conclusion

This work addresses the lack of interpretability in vision graph neural networks by introducing a novel inherently explainable ViG approach, called i-WiViG, which is capable of automatically identifying subgraphs containing the relevant long-range dependencies for the model prediction. We achieve this by first relying on graph layers that process local windows of the image and afterward by learning the global, long-range dependencies between the windows with the GSAT graph. While the local window processing constrains the receptive fields of the nodes to a local window in the image, the stochastic attention mechanism of GSAT graph layers explains the decision mechanism by assigning higher edge weights to the critical relations for the model prediction. We perform extensive quantitative and qualitative evaluations of our approach to classification and regression remote sensing tasks where long-range dependencies are typically present. The qualitative analysis indicates that our approach produces subgraphs that intuitively describe the model decision mechanism. For instance, our results show that the interpretable graph bottleneck emphasizes the connections between airplanes as most relevant for predicting the airplane class or that it identifies the connections from the residential area to a water body to derive the high liveability value. Further, we quantitatively demonstrate that these connections reliably represent the model workings. Finally, we also compare the explanation properties of our approach with the other state-of-the-art

ViG models with a quantitative post-hoc explanation evaluation which shows that i-WiViG reduces the infidelity of the explanations while at the same time producing comparative sparsity to the benchmarks. In summary, our work introduces an inherently interpretable ViG model that yields a competitive predictive performance to the state-of-the-art black-box ViG approaches while being capable of reliably explaining the decision patterns in terms of local and long-range interactions between the patches in the image.

References

- [1] Julius Adebayo, Justin Gilmer, Michael Muelly, Ian Goodfellow, Moritz Hardt, and Been Kim. Sanity checks for saliency maps. *Advances in neural information processing systems*, 31, 2018. 1, 3
- [2] Wieland Brendel and Matthias Bethge. Approximating cnns with bag-of-local-features models works surprisingly well on imagenet. *International Conference on Learning Representations*, 2019. 5
- [3] Boan Chen, Zhi Gao, Ziyao Li, Siqi Liu, Aohan Hu, Weiwei Song, Yu Zhang, and Qiao Wang. Hierarchical gnn framework for earth’s surface anomaly detection in single satellite imagery. *IEEE Transactions on Geoscience and Remote Sensing*, 2024. 1
- [4] Yongqiang Chen, Yatao Bian, Bo Han, and James Cheng. How interpretable are interpretable graph neural networks? In *Forty-first International Conference on Machine Learning*, 2024. 3
- [5] Gong Cheng, Junwei Han, and Xiaoqiang Lu. Remote sensing image scene classification: Benchmark and state of the art. *Proceedings of the IEEE*, 105(10):1865–1883, 2017. 5
- [6] Enmao Diao, Ganghua Wang, Jiawei Zhan, Yuhong Yang, Jie Ding, and Vahid Tarokh. Pruning deep neural networks from a sparsity perspective. *arXiv preprint arXiv:2302.05601*, 2023. 6, 8, 3
- [7] Robert Geirhos, Patricia Rubisch, Claudio Michaelis, Matthias Bethge, Felix A Wichmann, and Wieland Brendel. Imagenet-trained cnns are biased towards texture; increasing shape bias improves accuracy and robustness. In *International Conference on Learning Representations*, 2018. 1
- [8] Kai Han, Yunhe Wang, Jianyuan Guo, Yehui Tang, and Enhua Wu. Vision gnn: An image is worth graph of nodes. *Advances in neural information processing systems*, 35:8291–8303, 2022. 1, 2, 3, 4, 5
- [9] Yan Han, Peihao Wang, Souvik Kundu, Ying Ding, and Zhangyang Wang. Vision hgnn: An image is more than a graph of nodes. In *Proceedings of the IEEE/CVF International Conference on Computer Vision*, pages 19878–19888, 2023. 1, 2, 3
- [10] Kaiming He, Xiangyu Zhang, Shaoqing Ren, and Jian Sun. Deep residual learning for image recognition. In *Proceedings of the IEEE conference on computer vision and pattern recognition*, pages 770–778, 2016. 4, 5
- [11] Alex Levering, Diego Marcos, Jasper van Vliet, and Devis Tuia. Predicting the liveability of dutch cities with aerial images and semantic intermediate concepts. *Remote Sensing of Environment*, 287:113454, 2023. 5
- [12] Guohao Li, Matthias Muller, Ali Thabet, and Bernard Ghanem. Deepgcns: Can gcns go as deep as cnns? In *Proceedings of the IEEE/CVF international conference on computer vision*, pages 9267–9276, 2019. 1
- [13] Wanyu Lin, Hao Lan, Hao Wang, and Baochun Li. Orphicx: A causality-inspired latent variable model for interpreting graph neural networks. In *Proceedings of the IEEE/CVF Conference on Computer Vision and Pattern Recognition*, pages 13729–13738, 2022. 3
- [14] Qinghui Liu, Michael Kampffmeyer, Robert Jenssen, and Arnt-Børre Salberg. Self-constructing graph neural networks to model long-range pixel dependencies for semantic segmentation of remote sensing images. *International Journal of Remote Sensing*, 42(16):6184–6208, 2021. 1
- [15] Siqi Miao, Mia Liu, and Pan Li. Interpretable and generalizable graph learning via stochastic attention mechanism. In *International Conference on Machine Learning*, pages 15524–15543. PMLR, 2022. 1, 3, 4
- [16] Mustafa Munir, William Avery, and Radu Marculescu. Mobilevig: Graph-based sparse attention for mobile vision applications. In *Proceedings of the IEEE/CVF Conference on Computer Vision and Pattern Recognition*, pages 2211–2219, 2023. 1, 2, 3
- [17] Mustafa Munir, William Avery, Md Mostafijur Rahman, and Radu Marculescu. Greedyvig: Dynamic axial graph construction for efficient vision gnns. In *Proceedings of the IEEE/CVF Conference on Computer Vision and Pattern Recognition*, pages 6118–6127, 2024. 1, 2, 3
- [18] Meike Nauta, Jan Trienes, Shreyasi Pathak, Elisa Nguyen, Michelle Peters, Yasmin Schmitt, Jörg Schlötterer, Maurice Van Keulen, and Christin Seifert. From anecdotal evidence to quantitative evaluation methods: A systematic review on evaluating explainable ai. *ACM Computing Surveys*, 55(13s): 1–42, 2023. 7
- [19] Maxim Neumann, Andre Susano Pinto, Xiaohua Zhai, and Neil Houlsby. In-domain representation learning for remote sensing. *arXiv preprint arXiv:1911.06721*, 2019. 5
- [20] Vitali Petsiuk, Abir Das, and Kate Saenko. Rise: Randomized input sampling for explanation of black-box models. In *British Machine Vision Conference (BMVC)*, 2018. 6
- [21] Sara Sabour, Nicholas Frosst, and Geoffrey E Hinton. Dynamic routing between capsules. *Advances in neural information processing systems*, 30, 2017. 1
- [22] Gregory Scafarto, Madalina Ciortan, Simon Tihon, and Quentin Ferre. Augment to interpret: Unsupervised and inherently interpretable graph embeddings. In *Asian Conference on Machine Learning*, pages 1183–1198. PMLR, 2024. 3
- [23] Yuntao Shou, Wei Ai, Tao Meng, and Nan Yin. Graph information bottleneck for remote sensing segmentation. *arXiv preprint arXiv:2312.02545*, 2023. 1
- [24] Xinyang Song, Zhen Hua, and Jinjiang Li. Context spatial awareness remote sensing image change detection network based on graph and convolution interaction. *IEEE Transactions on Geoscience and Remote Sensing*, 2024. 1
- [25] Gabriele Spadaro, Marco Grangetto, Attilio Fiandrotti, Enzo Tartaglione, and Jhony H Giraldo. Wignet: Windowed vision

- graph neural network. *arXiv preprint arXiv:2410.00807*, 2024. [1](#), [2](#), [3](#), [4](#), [5](#)
- [26] Shuyang Sun, Jiangmiao Pang, Jianping Shi, Shuai Yi, and Wanli Ouyang. Fishnet: A versatile backbone for image, region, and pixel level prediction. *Advances in neural information processing systems*, 31, 2018. [5](#)
- [27] Mukund Sundararajan, Ankur Taly, and Qiqi Yan. Axiomatic attribution for deep networks. In *International conference on machine learning*, pages 3319–3328. PMLR, 2017. [6](#)
- [28] Tailin Wu, Hongyu Ren, Pan Li, and Jure Leskovec. Graph information bottleneck. *Advances in Neural Information Processing Systems*, 33:20437–20448, 2020. [4](#)
- [29] Keyulu Xu, Weihua Hu, Jure Leskovec, and Stefanie Jegelka. How powerful are graph neural networks? *arXiv preprint arXiv:1810.00826*, 2018. [1](#)
- [30] Chih-Kuan Yeh, Cheng-Yu Hsieh, Arun Suggala, David I Inouye, and Pradeep K Ravikumar. On the (in) fidelity and sensitivity of explanations. *Advances in neural information processing systems*, 32, 2019. [6](#)
- [31] Zhitao Ying, Dylan Bourgeois, Jiaxuan You, Marinka Zitnik, and Jure Leskovec. Gnnexplainer: Generating explanations for graph neural networks. *Advances in neural information processing systems*, 32, 2019. [1](#), [3](#)
- [32] Zhi-Hui You, Jia-Xin Wang, Si-Bao Chen, Chris HQ Ding, Gui-Zhou Wang, Jin Tang, and Bin Luo. Crossed siamese vision graph neural network for remote sensing image change detection. *IEEE Transactions on Geoscience and Remote Sensing*, 2023. [1](#)
- [33] Hao Yuan, Jiliang Tang, Xia Hu, and Shuiwang Ji. Xgnn: Towards model-level explanations of graph neural networks. In *Proceedings of the 26th ACM SIGKDD international conference on knowledge discovery & data mining*, pages 430–438, 2020. [3](#)
- [34] Hao Yuan, Haiyang Yu, Shurui Gui, and Shuiwang Ji. Explainability in graph neural networks: A taxonomic survey. *IEEE transactions on pattern analysis and machine intelligence*, 45(5):5782–5799, 2022. [3](#)
- [35] Sangdoon Yun, Dongyoon Han, Seong Joon Oh, Sanghyuk Chun, Junsuk Choe, and Youngjoon Yoo. Cutmix: Regularization strategy to train strong classifiers with localizable features. In *Proceedings of the IEEE/CVF international conference on computer vision*, pages 6023–6032, 2019. [1](#)
- [36] Cui Zhang, Liejun Wang, and Shuli Cheng. Hcgnet: A hybrid change detection network based on cnn and gnn. *IEEE Transactions on Geoscience and Remote Sensing*, 2024. [1](#)
- [37] Hongyi Zhang. mixup: Beyond empirical risk minimization. *arXiv preprint arXiv:1710.09412*, 2017. [1](#)

i-WiViG: Interpretable Window Vision GNN

Supplementary Material

A. i-WiViG Architecture

Table 4 presents in detail the layer composition and the hyperparameters used in our proposed i-WiViG model. Similar to the WiGNet and the pyramid ViG models, we perform a series of window grapher layers and downsampling layers. In contrast to these models and as illustrated in Table 1 in the main manuscript, we minimize the spatial overlap between the windows by using convolutions with kernel 2 and stride 2. Further, to obtain an inherently interpretable model that reveals the relevant subgraph for its prediction, we insert the GSAT graph in the final stage before the prediction head to learn the global long-range relations between the windows in the image by ranking the importance of the edges in the graph. Similar to the standard grapher layers in the ViG model, in the GSAT block we perform the operations in the following order to the graph node:

1. Linear transformation of the node embeddings
2. GIN graph convolution
3. Residual operation
4. FFN layer processing

Finally, the GSAT block is followed by a prediction head consisting of pooling and MLP layers, as illustrated in Table 4.

B. i-WiViG Training Procedure

For model training, we performed image transformations in the following order:

1. Resizing the images to a size of 256 x 256
2. Random Augmentation
3. Random Erasure
4. Min-max image normalization

Further, for the scene classification task, we have used the Cutmix [35] and Mixup [37] augmentations during training. Regarding the benchmark ViG models, we used the default hyperparameter setting of the tiny versions. For our i-WiViG model, we used the hyperparameters of the WiGNet grapher blocks illustrated in Table 4 setting while for the GSAT block, we used 4 layers.

C. Liveability Explanation Quality

In this section, we present additional experiments on liveability explanations. In Figure 8, we present the edge attribution evaluation when $r = 0.5$. It demonstrates that for the regression task, the edge weights typically have several orders of magnitude lower standard deviation and the explanation quality exhibits higher sensitivity to the choice of the r value with lower values linked to poorer explanation quality. Even

Table 4. **Detailed configuration of the i-WiViG model.** D: graph nodes feature dimension, E: hidden dimension ratio in FFN, k: number of neighbors in the GNN, W: window size, H x W: input image size. The WiGNet blocks use the Max-Relative Graph Conv operation [12] while the GSAT block uses the GIN Conv operation [29] for graph processing.

Stage	Output Size	Hyperparameters
Stem	$\frac{H}{4} \times \frac{W}{4}$	Conv \times 2
Stage 1		
WiGNet block	$\frac{H}{4} \times \frac{W}{4}$	$\begin{bmatrix} D = 48 \\ E = 4 \\ k = 9 \\ W = 4 \end{bmatrix} \times 2$
Downsample	$\frac{H}{8} \times \frac{W}{8}$	Conv \times 2
Stage 2		
WiGNet block	$\frac{H}{8} \times \frac{W}{8}$	$\begin{bmatrix} D = 96 \\ E = 4 \\ k = 9 \\ W = 4 \end{bmatrix} \times 2$
Downsample	$\frac{H}{16} \times \frac{W}{16}$	Conv \times 2
Stage 3		
WiGNet block	$\frac{H}{16} \times \frac{W}{16}$	$\begin{bmatrix} D = 240 \\ E = 4 \\ k = 9 \\ W = 4 \end{bmatrix} \times 4$
Downsample	$\frac{H}{32} \times \frac{W}{32}$	Conv \times 2
Stage 4		
GSAT block	$\frac{H}{32} \times \frac{W}{32}$	$\begin{bmatrix} D = 384 \\ E = 4 \\ k = 5 \end{bmatrix} \times 4$
Head	1×1	Pooling & MLP
Parameters (M)		17.4

though the AUC value is 0.46, we can see that when using $r = 0.5$, the edges do not faithfully explain the model as the R2 only varies slightly from 0.47 to around 0.4.

D. Post-Hoc Explanation Evaluation on the Liveability Task

Figure 9 visualize the effect of our proposed i-WiViG model on the quantitative xAI evaluation metrics for the IG and Occlusion attribution heatmaps on the Liveability regression task. Similar to the results for the infidelity metrics on the scene classification task in Figure visualized in 7.a, our i-WiViG approach produces comparable infidelity values to the Pyramid ViG and the WiGNet approach for both attribution methods. The infidelity of these models is much smaller compared to their infidelity on the scene classification task and significantly smaller than the isotropic ViG model for the regression task, which implies that the pyramid ViG models produce more reliable post-hoc explanations than

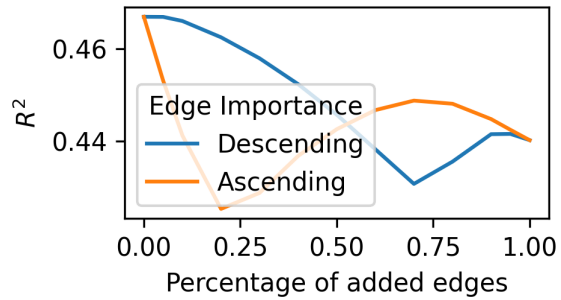
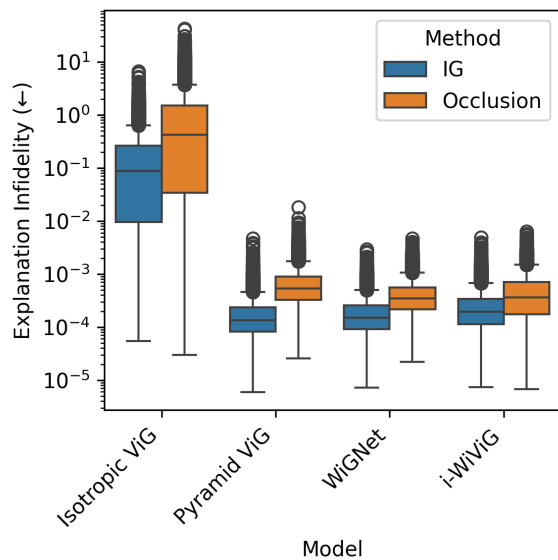
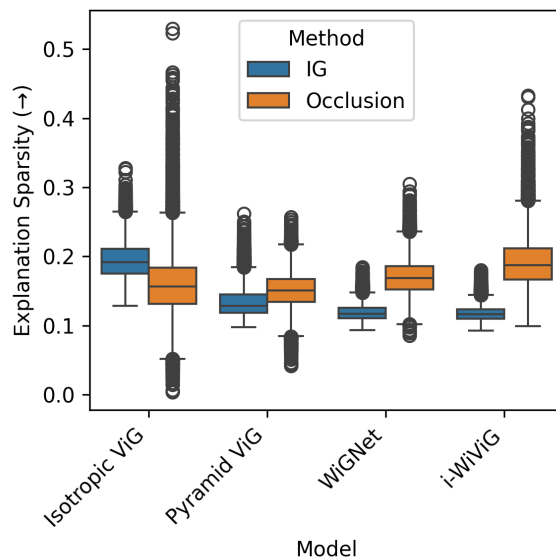


Figure 8. **Liveability edge attribution evaluation when using $r = 0.5$ for model training after an incremental addition of the edges with highest importance (blue curve) and the edges with lowest importance (orange curve).**

the isotropic ViG model. Further, the Occlusion attribution maps on Figure 9.b illustrate a similar trend to the sparsity results on the scene classification dataset as they yield on average slightly sparser explanations for the i-WiViG approach compared to the other ViG models. In contrast, the IG attributions illustrate an opposite trend as they are less sparse for our and the WiGNet approach than the Pyramid ViG and the isotropic ViG models.



(a) Explanation Infidelity



(b) Explanation Sparsity

Figure 9. **Quantitative evaluation of the explanation quality of our method against the other Vision GNN benchmarks on the Liveability regression dataset.** The left plot visualizes the explanation infidelity while the right plot depicts the explanation sparsity for the post-hoc attributions computed with the Integrated Gradients (IG) and Occlusion methods. The arrows indicate the preferred directions for the metrics, i.e. explanations with low fidelity and high sparsity are preferred. The explanation infidelity is visualized on the log scale while the sparsity was computed according to the PQ index [6].